Robust analysis of Demeter benchmark via quadratic separation ⋆

Dimitri Peaucelle * **Alberto Bortott** * **Frédéric Gouaisbaut** *,**
Denis Arzelier *

* *LAAS-CNRS ; Université de Toulouse ; 07 avenue Colonel Roche, F-31077 Toulouse, France, (e-mail: peaucell@laas.fr,arzelier@laas.fr).*
** *Université de Toulouse ; UPS, (e-mail: fgouaisb@laas.fr).*

Abstract: The purpose of this paper is to give numerical illustrations of recent results obtained in the area of robust analysis of uncertain parametric LTI systems. The idea is to highlight theoretical as well as numerical issues pertaining to real life applications of sophisticated robust analysis of spaceborne control systems. The framework of quadratic separation applied to interconnected implicit linear transformations and uncertain operators as defined in Peaucelle et al. (2007) is renewed. Improved robust stability tests involving more complex parameter-dependent Lyapunov functions are applied on a benchmark from the space industry. It is based on the problem of attitude control of a flexible satellite developed at CNES and it is used to analyze the relevance as well as some shortcomings of the proposed approach.

Keywords: Robust performance and stability analysis, LFT models, quadratic separation, attitude control, flexible satellite, benchmark.

1. INTRODUCTION

The main concerns of control system designers in the space industry are twofold. First, evaluate adequate and systematic methodologies for the design of multi-objective control systems for aerospace applications. Second, evaluate the potentiality of modern worst-case performance and stability analysis methods compared to the usual heavy and costly campaigns of parametric simulations. Indeed, physical systems from space industry are characterized by complex dynamics involving flexible structures and hardly modelled disturbances. As parametric uncertainty may affect the dynamics of the system as well as those of sensors and actuators (some of the parameters are not precisely known or may have different values on earth and on orbit), preliminary robust analysis of the proposed control laws is mandatory before its implementation on the real system. Despite the intensive and numerous studies of the community, robust stability and performance analysis of linear time-invariant (LTI) systems against parametric uncertainties is one of the most challenging problems from both theoretical and numerical points of view. This stage is nonetheless crucial since it allows to validate and to certify the performance of the control laws. Usually, *ad hoc* procedures based on gridding techniques or Monte Carlo simulations are specifically designed for each industrial application. These techniques are known to be reliable while not strictly guaranteeing the performance level. Moreover, they often lead to a heavy load of computation. On the contrary, methods defined in the context of robust control theory aim at providing a guaranteed but conservative level of performance whatever may be the parametric configuration of the plant.

A very complete SIMULINK simulator of the Attitude Control System (ACS) of the satellite Demeter (Pittet and Arzelier (2006)) including a linearized model of the satellite with associated models of parametric uncertainties, a model of the environment (disturbances torque), models of the actuators (reaction wheels and magneto-torquers) and an example of flight software, has been developed at CNES and has been proposed to the control community as a benchmark for both modern techniques of robust stability and performance analysis and robust control law synthesis. The purpose of this paper is to give numerical illustrations of recent results obtained in the area of robust analysis of uncertain parametric LTI systems using this benchmark. The idea is to highlight theoretical as well as numerical issues pertaining to real life applications of sophisticated robust analysis of spaceborne control systems. The framework of quadratic separation applied to interconnected implicit linear transformations and uncertain operators as defined in Peaucelle et al. (2007) is renewed and augmented by the results from Peaucelle (2009). Improved robust stability tests involving more complex parameter-dependent Lyapunov functions are applied on the Demeter benchmark. This realistic benchmark including modelling of three axis and four flexible modes is rich enough to analyze the relevance as well as the numerical shortcomings of the proposed approach.

2. UNCERTAIN LFT MODELS FOR THE BENCHMARK

First of all, an uncertain LTI model of the dynamics of the flexible satellite, the models for the sensor and the actuators, as well as the attitude control laws are needed in order to derive the complete uncertain model of the closed-loop system.

2.1 Satellite dynamics

The model for the dynamics of the satellite is a Linear Time Invariant (LTI) model composed of 3 double integrators scaled by inertia with four pairs of additional flexible modes (Pittet and Arzelier (2006)).

⋆ The authors are grateful to Christelle Pittet and CNES financially supported this study

$$\underbrace{\begin{bmatrix} A_1 & A_4 \\ A_4' & \mathbf{1}_8 \end{bmatrix}}_{M(\delta)} \begin{bmatrix} \delta\ddot{\theta} \\ \ddot{\eta} \end{bmatrix} = \underbrace{\begin{bmatrix} \mathbf{0} & \mathbf{0} \\ \mathbf{0} & C_s^- \end{bmatrix}}_{C_S(\delta)} \begin{bmatrix} \delta\dot{\theta} \\ \dot{\eta} \end{bmatrix} + \underbrace{\begin{bmatrix} \mathbf{0} & \mathbf{0} \\ \mathbf{0} & K_s^- \end{bmatrix}}_{K_S(\delta)} \begin{bmatrix} \delta\theta \\ \eta \end{bmatrix} + \begin{bmatrix} \mathbf{1} \\ \mathbf{0} \end{bmatrix} T_c \quad (1)$$

where $\delta\theta \in \mathbb{R}^3$ is the vector of pointing errors, $\eta \in \mathbb{R}^8$ is the state vector associated to flexible modes. A_1 and A_4 are respectively the matrix of inertia and the coupling matrix between $\delta\theta$ and the flexible modes composing the generalized mass matrix. The matrices $C_s^- = \mathrm{diag}(-2\xi_i\omega_i)$ and $K_s^- = \mathrm{diag}(-\omega_i^2),\ i = 1, \cdots, 8$ are diagonal generalized matrices of damping and stiffness respectively (Pittet and Arzelier (2006)). T_c is the control torque applied to the satellite. Some of the parameters of this LTI model are not precisely known or may have different values on earth and on orbit.

$\pm$ 30 % on the diagonal inertias I_{11}, I_{22}, I_{33}
$\pm$ 3 kg.m^2 on the off-diagonal inertias I_{12}, I_{13}, I_{23}
The damping ratios are such that $5\ 10^{-4} \leq \xi_i \leq 5\ 10^{-3},\ \forall\, i$
The natural frequencies are such that $0.2 * 2\pi$ rad/s $\leq \omega_i \leq 0.6 * 2\pi$ rad/s, $\forall\, i$
This results in an uncertain parameter vector with 14 independent entries $\delta = \left[\, \delta_{I_{ii}}\ \delta_{I_{ij}}\ \delta_{\xi_k}\ \delta_{\omega_k} \,\right]' \in \mathbb{R}^{14},\ i = 1, 2, 3,\ j = 2, 3,\ k = 1, \cdots, 4.$

Defining the state vector by $x = \left[\, \delta\theta\ \eta\ \delta\dot{\theta}\ \dot{\eta} \,\right]'$, we get the uncertain state-space model:

$$\begin{bmatrix} \delta\dot{\theta} \\ \dot{\eta} \\ \delta\ddot{\theta} \\ \ddot{\eta} \end{bmatrix} = \begin{bmatrix} \mathbf{0} & \mathbf{1} \\ M^{-1}K_S(\delta) & M^{-1}C_S(\delta) \end{bmatrix} \begin{bmatrix} \delta\theta \\ \eta \\ \delta\dot{\theta} \\ \dot{\eta} \end{bmatrix} + \begin{bmatrix} \mathbf{0} \\ M^{-1}(\delta) \begin{bmatrix} \mathbf{1} \\ \mathbf{0} \end{bmatrix} \end{bmatrix} U$$

$$\dot{x}(t) = A_{sat}(\delta)x(t) + B_{sat}(\delta)U \quad (2)$$

An uncertain LFT model of $A(\delta)$ and $B(\delta)$ is then derived from (2) using usual techniques and the LFR Toolbox Version 2.0 Magni (2005).

The final LFR $A_{sat}(\delta)$ is defined as:

$$A_{sat}(\delta) = A + B_\Delta \Delta_A \left(\mathbf{1}_{36} - D_{\Delta\Delta}\Delta_A\right)^{-1} C_\Delta \quad (3)$$

where $A \in \mathbb{R}^{22\times22}$, $D_{\Delta\Delta} \in \mathbb{R}^{36\times36}$ and

$$\Delta_A = \begin{bmatrix} \Delta_M & \mathbf{0}_{12\times24} \\ \mathbf{0}_{24\times12} & \Delta_{K_SC_S} \end{bmatrix} \quad (4)$$

$\Delta_{K_sC_s} = \mathrm{diag}_i\left(\delta_{\xi_i}\mathbf{1}_2, \delta_{\omega_i}\mathbf{1}_4\right),\ i = 1, \cdots, 4$. The final LFR $B_{sat}(\delta)$ may also be easily derived along the same lines but is not presented here since only robust analysis is dealt with.

2.2 Models of the actuators and the sensor

The satellite is actuated by three reaction wheels whose kinetic momentum is controlled by magneto-torquers. The behavior of the reaction wheels is considered to be a linear one represented by a second order low pass filter with saturations on the reference torque and its velocity.

The attitude sensor is a star tracker inducing a composite time delay for the measurements which are affected by noise and may not be available for feedback. The proposed linearized model is a $4th$ order Pade approximation defining a delay of 800 ms composed by a fixed delay of 300 ms, a varying delay of maximum equal to 400 ms and a 100 ms delay from the reaction wheels.

2.3 Flight software and control laws

During the mission, four different modes may be operated following specific requirements: Acquisition and safehold mode (MAS), coarse transition mode (MGT), normal mode (MNO) and orbit control mode (MCO). The scientific mission is performed during the normal mode requiring accurate pointing and therefore a particularly high level of performance and robustness for AOCS. The AOCS control loop during the normal mode is presented at figure 1. The flight software is composed of 3 rate estimators (one per axis), 3 filters and 3 composite nonlinear controllers built up from the large pointing error control laws and the small pointing error control laws. The formers must decrease the pointing errors when over a given threshold (due to transition initial conditions for instance) while the latter is required to ensure stability, pointing accuracy and robustness for small pointing errors.

The satellite angular velocity is derived from the star tracker attitude measurement via 3 high pass filters of first order, with a time constant of 0.5 seconds. They are digitalized at 4 Hz using bilinear transformation.

The reaction wheels control filters is composed of three parts: A nonlinear control law for large pointing error switching with a PD controller for small pointing errors, both followed by the same stabilizing linear filter. Here, for robustness analysis purpose, only the small pointing errors control is concerned.

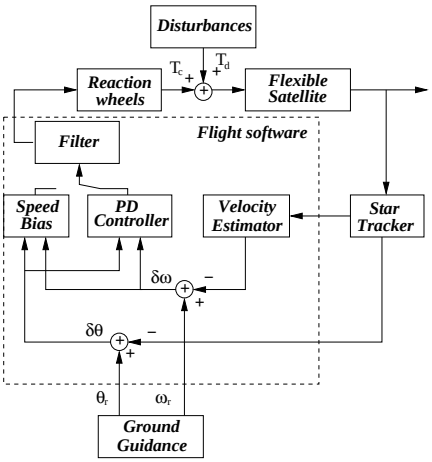

Fig. 1. Demeter MNO control loop

The small pointing errors control is applied under the pointing threshold. It must ensure the stability of the flexible and delayed satellite, the pointing accuracy, robustness regarding the model uncertainties, while respecting the reaction wheels capacity and providing a smooth switch with the speed bias law.

$$T_i = -Kp_i \times \delta\theta_{esti} - Kd_i \times \delta\omega_{esti},\ i = 1, \ldots, 3 \quad (5)$$

where Kp_i and Kd_i are respectively the proportional and derivative gains on axis i. For Demeter, the values are $Kp_1 = Kp_2 = Kp_3 = 20$, $Kd_i = 20Kp_i$ and the threshold is 0.3 deg on X and Z axis, and 0.5deg on Y axis.

The synthesis of the stabilizing filter will not be detailed here. The 3 SISO control filters are the result of a multi-objective H_2/H_∞ LMI synthesis with pole placement in a LMI region. Some information about the synthesis can be found in Pittet et al. (2001).

3. ROBUST ANALYSIS VIA QUADRATIC SEPARATION FOR IMPLICIT INTERCONNECTIONS

As our main objective is to give numerical results related to the specific application of modern robust analysis to ACS of Demeter, only the major lines of developments of the theoretical results used here are recalled. For a more detailed exposition, the reader may have a look at the references Iwasaki and Hara (1998), Peaucelle and Arzelier (2001), Iwasaki and Shibata (2001), Peaucelle et al. (2007) (see also Safonov (1980) for a thorough presentation of topological separation).

3.1 Augmented implicit formulation

Remember that $A_{sat}(\delta)$ representing the dynamics of the satellite depends rationnally upon the uncertain parameters and therefore may be represented as the following interconnection:

$$\begin{pmatrix} \dot{x} \\ z_\Delta \end{pmatrix} = \begin{bmatrix} A & B_\Delta \\ C_\Delta & D_{\Delta\Delta} \end{bmatrix} \begin{pmatrix} x \\ w_\Delta \end{pmatrix}, \quad w_\Delta = \Delta_A z_\Delta \qquad (6)$$

Robust analysis of uncertain model (6) may be performed using well-posedness (equivalent to robust stability) of the interconnection of the uncertain operator and the nominal system matrices and by applying usual quadratic separation results from Iwasaki and Shibata (2001) and Peaucelle and Arzelier (2001). For structured uncertain operators, the choice for the quadratic separator is a key point to get effective stability tests that give an acceptable trade-off between numerical tractability and reduction of conservatism. A complementary way to tackle this difficult issue has been proposed in Iwasaki and Shibata (2001) and extended in Ebihara et al. (2005). The idea is to include additional information in the interconnection by considering derivatives of some internal signals. This results in a new interconnection possibly involving implicit transformations. For instance, we have:

$$\dot{w}_\Delta = \Delta \dot{z}_\Delta + \dot{\Delta} z_\Delta = \Delta \dot{z}_\Delta \qquad (7)$$

for the uncertain model (6), assuming that the uncertainty operator Δ is time-invaraint (parametric constant uncertainty in the case od Demeter). Deriving all necessary relations describing the interconnection and the available information leads to the augmented uncertain descriptor model.

$$\overbrace{\left[\begin{array}{cc|cc} \mathbf{0} & \mathbf{0} & \mathbf{1} & \mathbf{0} \\ \mathbf{1} & \mathbf{0} & \mathbf{0} & \mathbf{0} \\ \mathbf{0} & \mathbf{1} & \mathbf{0} & \mathbf{-1} \\ \mathbf{0} & \mathbf{0} & \mathbf{1} & \mathbf{0} \\ -C_\Delta & \mathbf{0} & \mathbf{0} & \mathbf{1} \end{array}\right]}^{\mathcal{E}} \overbrace{\left(\begin{array}{c} \dot{x} \\ \hline \dot{z}_\Delta \\ z_\Delta \\ \dot{z}_\Delta \end{array}\right)}^{z} = \overbrace{\left[\begin{array}{cc|cc} \mathbf{0} & \mathbf{1} & \mathbf{0} & \mathbf{0} \\ A & \mathbf{0} & B_\Delta & \mathbf{0} \\ \mathbf{0} & \mathbf{0} & \mathbf{0} & \mathbf{0} \\ C_\Delta & \mathbf{0} & D_{\Delta\Delta} & \mathbf{0} \\ \mathbf{0} & \mathbf{0} & \mathbf{0} & D_{\Delta\Delta} \end{array}\right]}^{\mathcal{A}} \overbrace{\left(\begin{array}{c} x \\ \hline z_\Delta \\ w_\Delta \\ \dot{w}_\Delta \end{array}\right)}^{w}$$

$$\begin{aligned} w_\Delta &= \Delta z_\Delta \\ \dot{w}_\Delta &= \Delta \dot{z}_\Delta + \dot{\Delta} z_\Delta = \Delta \dot{z}_\Delta \end{aligned} \qquad (8)$$

Robust stability of (8) is now equivalent to the well-posedness of the interconnection of figure 2 (Peaucelle et al. (2009)).

Definition 1. The interconnection of the figure 2 is *well-posed* if for all bounded $(\bar{z}, \bar{w})$ s.t. :

$$\mathcal{E} z(t) = \mathcal{A} w(t) + \bar{w}(t), \; w(t) = [\nabla z](t) + \bar{w}(t) \qquad (9)$$

and for all admissible $\nabla \in \boldsymbol{\nabla}$, the signals $(\mathcal{E}z, w)$ are unique and bounded :

$$\exists \bar{\gamma} > 0 \;\; : \;\; \left\| \begin{matrix} \mathcal{E}w \\ w \end{matrix} \right\| \leq \bar{\gamma} \left\| \begin{matrix} \bar{z} \\ \bar{w} \end{matrix} \right\| \;\; , \;\; \begin{matrix} \forall \begin{pmatrix} \bar{z} \\ \bar{w} \end{pmatrix} \in \mathcal{L}_2 \\ \forall \nabla \in \boldsymbol{\nabla} \end{matrix} \; . \qquad (10)$$

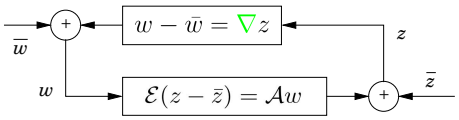

Fig. 2. Implicit interconnection for the augmented model

where $\nabla = \begin{bmatrix} \mathcal{I}_{n+m} & \mathbf{0} & \mathbf{0} \\ \mathbf{0} & \Delta & \mathbf{0} \\ \mathbf{0} & \mathbf{0} & \Delta \end{bmatrix} \in \boldsymbol{\nabla}$, $\mathcal{I}$ is the integral operator, $\mathcal{I} \; : \; x(t) \rightarrow \int_0^t x(s)ds$ and $\boldsymbol{\nabla}$ is the domain of the operator ∇. $\|f\| = < f|f >$ where $< f|g >=$ Trace $\left(\int_0^\infty f^*(t)g(t)dt\right)$ stands for the scalar product defined in the Hilbert space $\mathcal{L}_2$ of square integral functions. As will be seen in the sequel, this procedure of derivation and augmentation may be performed once again and so on (`index` is the order of derivation in the sequel), adding new information at each step that will allow to get a reduction of the derived robust stability tests at the expense of more numerical involved computations.

A general result for the well-posedness of the interconnection of figure 2 is now recalled.

3.2 Well-posedness of implicit interconnections

Let us consider the interconnection of figure 2 defined by the equations:

$$\mathcal{E} z(t) = \mathcal{A} w(t) \;\; , \;\; w(t) = [\nabla z](t) \qquad (11)$$

where $\mathcal{E}$ and $\mathcal{A}$ are possibly non square constant matrices. ∇ is a possibly non causal operator belonging to a domain $\nabla \in \boldsymbol{\nabla}$.

Theorem 1. Peaucelle et al. (2009)

Let $\mathcal{E} = \mathcal{E}_1 \mathcal{E}_2$ be a factorization of the matrix $\mathcal{E}$ where $\mathcal{E}_1$ is full-column rank. The interconnection of the figure 2 is well-posed it there exists a Hermitian matrix Θ simultaneously satisfying the following Linear Matrix Inequality (LMI) :

$$[\, \mathcal{E}_1 \;\; -\mathcal{A} \,]^{\perp *} \, \Theta \, [\, \mathcal{E}_1 \;\; -\mathcal{A} \,]^{\perp} > \mathbf{0} \qquad (12)$$

and the Integral quadratic Constraint:

$$\left\langle \begin{pmatrix} \mathcal{E}_2 z \\ \nabla z \end{pmatrix} \middle| \Theta \begin{pmatrix} \mathcal{E}_2 z \\ \nabla z \end{pmatrix} \right\rangle \leq 0 \;\; , \;\; \begin{matrix} \forall z \in \mathcal{L}_2 \\ \forall \nabla \in \boldsymbol{\nabla} \end{matrix} \; . \qquad (13)$$

where $A^\perp$ spans the kernel of A.

This result is a generalization of the well-known result on quadratic separation from Iwasaki and Shibata (2001) and has strong relationships with robust analysis techniques developed in the IQC framework (Megreski and Rantzer (1997)) and to the full-block S-procedure (Scherer (1997)). The key issue concerning theorem 1 is our capacity to translate the existence conditions (12), (13) into effective and constructive (with respect to the separator Θ) tests expressed in terms of LMI. In theorem 1, the inequality (12) is an LMI with respect to Θ when (13) is a more complex inequality to handle on the continuum $\boldsymbol{\nabla}$. The next subsection proposes some finite convex relaxations for the construction of quadratic separator verifying (13) and denoted admissible quadratic separator for (13).

3.3 LMIs for quadratic separation and Parameter-dependent Lyapunov functions

The operator ∇ may be built up as a sum of elementary operators ($\nabla_j \in \boldsymbol{\nabla}_j$), $\nabla = \sum_{j=1}^{\bar{\jmath}} J_j \nabla_j K_j$ where matrices J_j are such that ($J_{j_1}^* J_{j_2} = \mathbf{0}$ if $j_1 \neq j_2$ and $J_j^* J_j = \mathbf{1}$). Note that an LMI representation $\mathcal{L}(\boldsymbol{\nabla}_j)$ of admissible elementary quadratic separators (verifying inequality (13) on $\boldsymbol{\nabla}_j$) is available in many cases (integrator, polytopic uncertainties, see a more complete list in Peaucelle et al. (2009)). Let us define the following matrices:

$$L_j = K_j^{\perp} \quad , \quad G_j = (L_j^* \mathcal{E}_2^*)^{\perp} \quad , \quad F_j = K_j \mathcal{E}_2^* G_j \ . \tag{14}$$

and the notation $A^{\circledast} = A^{*\circ}$ where $\left[\begin{array}{cc} A^{\perp} & A^{\circledast} \end{array}\right]$ spans $\mathbb{C}^m$ for $A \in \mathbb{C}^{n \times m}$. We get the following relaxation:

Theorem 2. Peaucelle (2009)
If $\Theta_1, \ldots \Theta_{\bar{\jmath}}$ are respectively admissible quadratic separators for the elementary operators $\nabla_1, \ldots, \nabla_{\bar{\jmath}}$, i.e.

$$\Theta_j \in \mathcal{L}(\boldsymbol{\nabla}_j) \tag{15}$$

then, for all $\Psi_1, \ldots \Psi_{\bar{\jmath}}$ verifying the following LMIs:

$$\left[\begin{array}{cc} F_j F_j^{\circledast} & \mathbf{0} \\ \mathbf{0} & \mathbf{1} \end{array}\right] \Psi_j \left[\begin{array}{cc} F_j F_j^{\circledast} & \mathbf{0} \\ \mathbf{0} & \mathbf{1} \end{array}\right]^* \leq \Theta_j \tag{16}$$

and for all matrix Y, the following Θ:

$$\Theta = \left[\begin{array}{c} {\mathcal{E}_2}^{*\perp} \\ \mathbf{0} \end{array}\right] Y + Y^* \left[\begin{array}{c} {\mathcal{E}_2}^{*\perp} \\ \mathbf{0} \end{array}\right]^* + \sum_{j=1}^{\bar{\jmath}} \left[\begin{array}{cc} G_j F_j^{\circledast} & \mathbf{0} \\ \mathbf{0} & J_j \end{array}\right] \Psi_j \left[\begin{array}{cc} G_j F_j^{\circledast} & \mathbf{0} \\ \mathbf{0} & J_j \end{array}\right]^* \tag{17}$$

is an admissible quadratic separator satisfying (13).

Corollary 1. Peaucelle (2009)
If there exists a quadratic separator

$$\Theta \in \mathcal{L}(\boldsymbol{\nabla}) \, \{ \, \Theta \ : \ (15), (16), (17) \ \} \tag{18}$$

verifying (12) then the interconnection of figure 2 is well-posed.

Note that the conservatism of the proposed robust analysis LMI tests mainly comes from the LMI description of admissible quadratic separators.

An important point to mention is that the robust stability tests based on quadratic separation and augmented uncertain model naturally exhibits Lyapunov certifcates of robust stability ranging from a parameter independent Lyapunov function (`index=0` for quadratic stability) to more involved parameter-dependent Lyapunov functions (`index>0`). This fact clearly explains the reduction of the conservatism noticed in the proposed application. For instance, the Lyapunov certificate for (6) with one step of derivation (implicit model (8)) and the application of quadratic separation results is given by the following parameter-dependent Lyapunov function (Iwasaki and Shibata (2001)):

$$P(\Delta) = \left[\begin{array}{cc} \mathbf{1} & \Delta_C^T \end{array}\right] \left[\begin{array}{cc} P_{11} & P_{12} \\ P_{12}^T & P_{22} \end{array}\right] \left[\begin{array}{c} \mathbf{1} \\ \Delta_C \end{array}\right] \tag{19}$$

$$\Delta_C = \Delta(\mathbf{1} - D_{\Delta\Delta}\Delta)^{-1} C_{\Delta}$$

4. NUMERICAL RESULTS

Robust analysis of the benchmark Demeter follows two different stages. In the first one, the parametric domain of uncertainty is fixed and normalized, considering that each parameter belongs to the interval $[-1, 1]$. For this step, uncertain models of increasing complexity are analysed. Indeed, for numerical reasons, it seems impossible to tackle directly the robust analysis problem for the complete uncertain description of the flexible multi-axis satellite. At our knowledge, no existing guaranteed robust analysis method could deal with such a large-scale uncertain model in a reasonable computation time.

4.1 Robust analysis for fixed uncertainty domains

Three axis model without flexible modes For this uncertain model $A_{sat}(\delta) \in \mathbb{R}^{27 \times 27}$ with $\delta \in \mathbb{R}^6$ and $\Delta_A \in \mathbb{R}^{9 \times 9}$. This uncertain model is proved not to be quadratic stable (a single Lyapunov certificate independent of the parameters cannot prove the robust stability) while the proposed robust stability test based on quadratic separation with `index=1` (parameter-dependent Lyapunov function of the form (19)) guarantees the robust stability of the closed-loop uncertain multi-axis rigid model of the satellite. Uncertain models for each axis with one additional flexible mode are now considered.

Axis i with one flexible mode For each axis i, the uncertain model is such that $A_{sat}(\delta) \in \mathbb{R}^{11 \times 11}$ with $\delta \in \mathbb{R}^3$ and $\Delta_A \in \mathbb{R}^{6 \times 6}$. As will be seen in the next subsection, this reduced uncertain model is useful to illustrate the relevance of the approach since plots of 3D safe domains may be easily done. Applying the quadratic separation robust stability test based on the parameter-dependent certificate (19), we get that axis 2 with one flexible mode is robustly stable while the test fails for the two other axis 1 and 3. In these last two cases, not only the conservatism of the approach leads to this result. Indeed, a quick analysis of the uncertain domain of the first axis with one flexible mode allows to exhibit destabilizing realizations of the parameters: $\delta J_{11} = 0, \delta\omega_1 = 1, \delta\xi_1 = -0.9$.

These preliminary results indicate that a more precise robust stability analysis on one axis with one flexible mode has to be performed to identify safe domains of the ACS in the uncertain parameters space. In the next section, the uncertain model of the first axis with one flexible mode is considered.

4.2 Heuristic construction of safe uncertainty domains

Here, $\delta = \left[\begin{array}{ccc} \delta J_{11} & \delta\omega_1 & \delta\xi_1 \end{array}\right]' \in \mathbb{R}^3$ and our goal is to build the safe domain in the hypercube $\mathcal{C} = [-1, 1] \times [-1, 1] \times [-1, 1]$ of the parametric space. Without a priori knowledge on the geometry of the safe domain and willing to find a trade-off between the size of the domain and the computational time, an iterative LMI-based bisection heuristic has been defined to build safe polytopes centered at the origin of $\mathcal{C}$.

1- Build an initial safe polytope $\mathcal{P}_0$ equal to a hypercube centered at the origin of $\mathcal{C}$. $\mathcal{P}_i = \mathcal{P}_0$
2- Number the 2^p vertices of the polytope $\mathcal{P}_i$.
3- For each vertex in the order of numbering, find a new safe vertex in the direction of the vertex of the hypercube $\mathcal{C}$ replacing the previous one.
4- Build the new polytope $\mathcal{P}_{i+1}$. $i \leftarrow i + 1$. Repeat 3 until the distance between feasbility and non feasability reaches some precision level.

Safe domains in 2D for fixed δJ_{11} This procedure is first illustrated in 2D with a frozen δJ_{11} and safe domains are represented at figures 3, 4 and 5. A gridding (red points with a step of 0.05) of the non safe realizations has been added to visualize the safe domains.

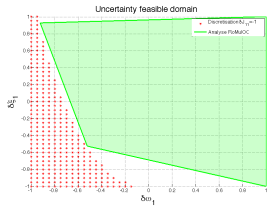

Fig. 3. Safe domain for $\delta J_{11} = -1$

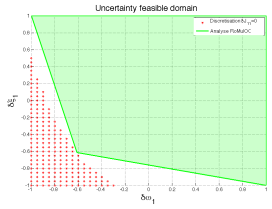

Fig. 4. Safe domain for $\delta J_{11} = 0$

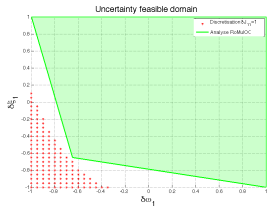

Fig. 5. Safe domain for $\delta J_{11} = 1$

Figures 3, 4 and 5 mainly show that the procedure succeeds in finding non conservative polytopes with 4 vertices with `index=1`. This result should be compared to the one obtained with an identical procedure based on quadratic stability test (`index=0`) at figure 6 ($-0.008 \leq \delta\omega_1 \leq 0.006$ and $-0.01 \leq \delta\xi_1 \leq 0.01$).

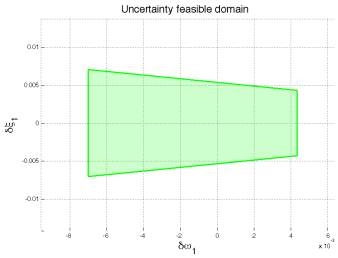

Fig. 6. Safe polytope for a single Lyapunov function

Safe domains in 3D The procedure described above is now used in the case where $\delta = \left[\, \delta J_{11} \;\; \delta\omega_1 \;\; \delta\xi_1 \,\right]'$. In the first tests, the quadratic separation tests are performed as in Iwasaki and Hara (1998) or Peaucelle and Arzelier (2001) and coded in the toolbox RoMulOC (Peaucelle and Arzelier (2006)), without the descriptor formulation described here and implicitly corresponds to the choice `index=1`. As indicated by figure 7, vertices 1 and 5 are the limiting ones as they are almost on the boundary of the unsafe domain.

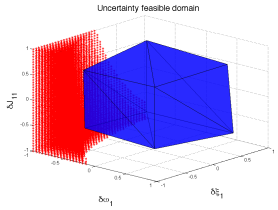

Fig. 7. Polytope of safe parameters

Figure 7 clearly shows that the chosen heuristic tries to expand the original polytope while keeping a geometry close the one of an hypercube. No direction is given a particular priority in the process of expansion. This is to be compared to a different procedure for which some directions are randomly favored. Four instances of this randomization of the heuristic algorithm are plot at figure 8. The union of these safe polytopes form a safe domain.

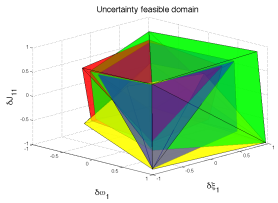

Fig. 8. Safe polytope with random directions

The final robust stability results are obtained using the augmented formulation and quadratic separation of the associated interconnection of figure 2 for increasing order of the parameter-dependent Lyapunov certificate: `index=0` (figure 9), `index=1` (figure 10), `index=2` (figure 11) and `index=3` (figure 12).

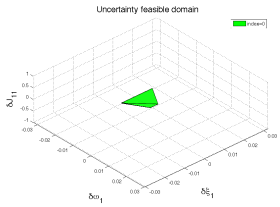

Fig. 9. Safe polytope for `index=0`

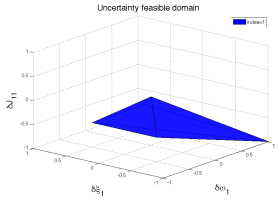

Fig. 10. Safe polytope for `index=1`

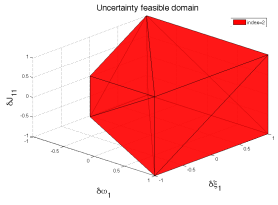

Fig. 11. Safe polytope for `index=2`

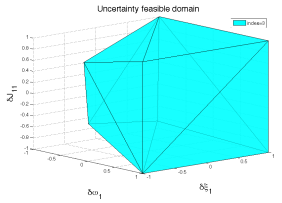

Fig. 12. Safe polytope for `index=3`

Here, the heuristic algorithm that has been used is slightly different from the previous since the distance to the next feasible vertex in the direction computed for the first vertex is maximized. The shape of the polytopes presented in the figures 9, 10, 11, 12 is in general more flat than in the previous experiments. The reduction of the conservatism of the obtained safe domains is quite spectacular for `index=2` and `index=3`. Comparisons of the computed critical vertices for these two cases are given in table 1 showing the sensible improvement from `index=2` to `index=3`. Finally, some information about the numerical

Table 1. Vertices for `index=2` and `index=3`

index=2			index=3		
δJ_{11}	$\delta\omega_1$	$\delta\xi_1$	δJ_{11}	$\delta\omega_1$	$\delta\xi_1$
-0.5156	-0.5156	-0.5156	-0.5312	-0.5312	-0.5312
-0.6562	-0.6562	0.6562	-0.7812	-0.7812	0.7812
0.5156	-0.5156	-0.5156	0.5703	-0.5703	-0.5703

complexity attached to the proposed robust stability tests are given in the table 2. Note that a preliminary version of these tests are coded in the last evolution of RoMulOC named Romuald using the LMI parser Yalmip Löfberg (2004) and the LMI solver SeDuMi Sturm (1999).

Table 2. Numerical complexity and size of LMIs

`index`	nb vars	dim LMI	solve LMI	find polytope
0	216	949×949	0.3s	113s
1	646	2754×2754	3s	746s
2	1614	6185×6185	25s	793s
3	3024	11050×11050	204s	3859s

5. CONCLUSIONS

Some promising numerical results for guaranteed robust analysis have been obtained on a non trivial ACS for a flexible satellite using most recent theoretical results of quadratic separation. Additional numerical advances are nevertheless required since only subclasses of the original robust analysis problem may be dealt with. A major interest of the proposed approach relies on the underlying unifying setup that allows to tackle different robust analysis problems with the same tools. Indeed, Robust performance (H_∞, H_2 or impulse-to-peak (Peaucelle et al. (2009))) as well as robustness with respect to delays in the loop (see Gouaisbaut and Peaucelle (2007) and the references therein) could be easily tackled in this framework.

REFERENCES

Ebihara, Y., Peaucelle, D., Arzelier, D., and Hagiwara, T. (2005). Robust performance analysis of linear time-invariant uncertain systems by taking higher-order time-derivatives of the states. In *joint IEEE Conference on Decision and Control and European Control Conference*. Seville, Spain. In Invited Session "LMIs in Control".

Gouaisbaut, F. and Peaucelle, D. (2007). Robust stability of time-delay systems with interval delays. In *IEEE Conference on Decision and Control*. New Orleans.

Iwasaki, T. and Hara, S. (1998). Well-posedness of feedback systems: Insights into exact robustness analysis and approximate computations. *IEEE Trans. on Automat. Control*, 43(5), 619–630.

Iwasaki, T. and Shibata, G. (2001). LPV system analysis via quadratic separator for uncertain implicit systems. *IEEE Trans. on Automat. Control*, 46(8), 1195–1207.

Löfberg, J. (2004). YALMIP3. `http://control.ee.ethz.ch/~joloef/yalmip.msql`.

Magni, J. (2005). User manual of the linear fractional representation toolbox version 2.0. Technical report, ONERA - Systems Control and Flight Dynamics Depertment. URL: `www.cert.fr/dcsd/idco/perso/Biannic%verb+/toolboxes.html+`.

Megreski, A. and Rantzer, A. (1997). System analysis via integral quadratic constraints. *IEEE Trans. on Automat. Control*, 42(6), 819–830.

Peaucelle, D. (2009). Integral quadratic separation applied to polytopic systems. In *IFAC Symposium on Robust Control Design*. Haifa.

Peaucelle, D. and Arzelier, D. (2001). Robust performance analysis with LMI-based methods for real parametric uncertainty via parameter-dependent Lyapunov functions. *IEEE Trans. on Automat. Control*, 46(4), 624–630.

Peaucelle, D. and Arzelier, D. (2006). Robust multi-objective control toolbox. In *IEEE International Symposium on Computer-Aided Control Systems Design*. Munich.

Peaucelle, D., Arzelier, D., Henrion, D., and Gouaisbaut, F. (2007). Quadratic separation for feedback connection of an uncertain matrix and an implicit linear transformation. *Automatica*, 43, 795–804. Doi: 10.1016/j.automatica.2006.11.005.

Peaucelle, D., Baudouin, L., and Gouaisbaut, F. (2009). Integral quadratic separators for performance analysis. In *European Control Conference*. Budapest.

Pittet, C., , and Fallet, C. (2001). Gyroless attitude control of a flexible microsatellite. In *DCSSS02 (5th conference on Dynamics and Control of Systems and Structures in Space)*. Cambridge, UK.

Pittet, C. and Arzelier, D. (2006). Demeter: A benchmark for robust analysis and control of the attitude of flexible micro satellites. In *IFAC Symposium on Robust Control Design, ROCOND'06*. Toulouse, France.

Safonov, M. (1980). *Stability and Robustness of Multivariable Feedback Systems*. Signal Processing, Optimization, and Control. MIT Press.

Scherer, C. (1997). A full block S-procedure with applications. In *IEEE Conference on Decision and Control*, 2602–2607. San Diego, CA.

Sturm, J. (1999). Using SeDuMi 1.02, a MATLAB toolbox for optimization over symmetric cones. *Optimization Methods and Software*, 11-12, 625–653. URL: `http://sedumi.mcmaster.ca/`.